JBC Papers in Press. Published on April 4, 2016 as Manuscript M116.722470
The latest version is at http://www.jbc.org/cgi/doi/10.1074/jbc.M116.722470

Electrogenic steps associated with substrate binding to the neuronal glutamate transporter EAAC1

Rose Tanui[1], Zhen Tao[2], Nechama Silverstein[3], Baruch Kanner[3]and Christof Grewer[1]

[1]Department of Chemistry Binghamton University, Binghamton, NY 13902

[2]Current address: 14323 Woodcrest Drive, Rockville, MD 29853

[3]Department of Biochemistry and Molecular Biology, Institute for Medical Research Israel-Canada Faculty of Medicine, Hebrew University, Jerusalem 91120, Israel.

Running title: *Electrogenic substrate binding to glutamate transporters*

To whom the correspondence should be addressed: Christof Grewer, [1]Department of Chemistry Binghamton University, 4400 Vestal Pkwy East, Binghamton, NY 13902, Phone: 607-777-3250, Fax: 607-777-4478, e-mail: cgrewer@binghamton.edu

Keywords: Glutamate transporter, mutagenesis, electrophysiology, kinetics, mechanism, simulations

ABSTRACT

Glutamate transporters actively take up glutamate into the cell, driven by the co-transport of sodium ions down their transmembrane concentration gradient. It was proposed that glutamate binds to its binding site and is subsequently transported across the membrane in the negatively charged form. With the glutamate binding site being located partially within the membrane domain, the possibility has to be considered that glutamate binding is dependent on the transmembrane potential, and, thus, electrogenic. Experiments presented in this report test this possibility. Rapid application of glutamate to the wild-type glutamate transporter subtype EAAC1 (excitatory amino acid carrier 1) through photo-release from caged glutamate generated a transient inward current, as expected for the electrogenic inward movement of co-transported Na^+. In contrast, glutamate application to a transporter with the mutation A334E induced transient outward current, consistent with movement of negatively-charged glutamate into its binding site within the dielectric of the membrane. These results are in agreement with electrostatic calculations, predicting a valence for glutamate binding of -0.27. Control experiments further validate and rule out other possible explanations for the transient outward current. Electrogenic glutamate binding can be isolated in the mutant glutamate transporter because reactions such as glutamate translocation and/or Na^+ binding to the glutamate-bound state, are inhibited by the A334E substitution. Electrogenic glutamate binding has to be considered together with other voltage dependent partial reactions to cooperatively determine the voltage dependence of steady-state glutamate uptake and glutamate buffering at the synapse.

Plasma membrane glutamate transporters of the solute carrier 1 (SLC1) family actively take up glutamate from the extracellular space (1-2). The uptake process is energetically driven by the co-transport of three Na^+ ions and one proton, as well as the counter-transport of one K^+ ion (3-4). Binding of at least two of these Na^+ ions has been shown to be dependent on the transmembrane potential, indicating that the cation binding sites are located at least somewhat within the membrane dielectric (5-6). This idea is consistent with the available structural and computational data, showing that the Na1 binding site, as well as

the predicted Na3' sites are located close to the midpoint of the membrane (7-8). Electrogenic Na^+ binding appears to be a hallmark of many Na^+-driven, secondary-active transporters, and has been also demonstrated for glucose transporters (9), GABA transporters of the SLC6 family (10), amino acid transporters (11), and phosphate transporters (12).

Several reports have indicated that glutamate is transported in its negatively-charged form, in which its carboxy side chain is deprotonated (13-14). The main evidence comes from mutagenesis studies, implying a conserved arginine residue in the binding site, R446 (EAAC1 sequence numbering) in the formation of a salt bridge with the γ-carboxylate of the glutamate substrate bound to the transporter (15). This idea was confirmed by the structure of the archeal glutamate transporter homologue Glt_{Ph} (16). In this structure, the bound substrate, aspartate, is located in a binding site that is protected from the extracellular side of the membrane by hairpin loop 2 (HP2), thus locking the substrate into the binding site. Access to the binding site appears to only be possible when HP2 opens, allowing the substrate to bind and/or dissociate (16). This structural picture suggests that substrate binding and/or occlusion occurs part way through the membrane electric field, which would result in electrogenic binding of a negatively-charged amino acid. However, to date no experimental evidence for electrogenic substrate binding has been obtained.

In this report, we provide results from a mutant glutamate transporter, in which substrate translocation and/or Na^+ binding to the glutamate-bound form is/are slowed down, but which still allows for glutamate binding. The mutated amino acid residue, A334E, is located at the tip of HP1 (Fig. 1A), which was previously implied to act as the internal gate (16), and is also important in Na^+ coordination. The mutation was originally designed to test structural changes involving HP1 during translocation, by engineering charge movement through the introduction of negative charge. However, our results suggest that the charge-altering mutation electrostatically interferes with structural changes and sodium binding to the glutamate-bound transporter, allowing us to isolate substrate binding, and steps associated with it, along the time axis. We demonstrate outward charge movement upon rapid glutamate application to the A334E mutant transporter, which is consistent with an electrogenic glutamate binding step and/or structural changes induced by glutamate binding. The experimental results are compared with computational analysis of the electrostatics of glutamate binding/HP2 closure, which also suggest that binding is voltage-dependent. Kinetic and structural models are proposed to explain the data and to exclude other possible mechanisms of glutamate-induced outward currents.

EXPERIMENTAL PROCEDURES

Molecular Biology, Cell culture and transfection. HEK293 cells (American Type Culture Collection No. 1573) were cultured as previously described (6). Sub confluent cell cultures were transiently transfected with EAAC1 cDNA inserted into a pBK-CMV-expression plasmid by use of JETPRIME Transfection reagent, following the protocol provided by the manufacturer. The cells were then used for electrophysiological measurements 24 hours after transfection. Site-directed mutagenesis was performed using the Quikchange method, as detailed in the manufacturer's protocol (Stratagene).

Whole-cell current recording. Whole-cell currents from EAAC1-expressing cells were recorded using an Adams& List EPC7 amplifier under voltage-clamp conditions (17). The typical resistance of the recording electrode was 2-3 MΩ; the series resistance was 5-8MΩ. For recordings performed under steady state conditions, the glutamate-induced currents were small (typically<500 pA). Therefore, series resistance was not compensated. For voltage jump experiments, series resistance compensation of 40-50% was applied in order to accelerate the capacitive charging of the membrane in response to the changes of the membrane potential (18).

All currents were low pass filtered at 1-10 kHz (KROHN-Hite 3200), and digitized with a digitizer board (Axon, Digidata 1200) at a sampling rate of 10-50 kHz, which was controlled by software (Axon PClamp). The experiments were carried out at room temperature and physiological pH.

The rapid solution exchange experiments were carried out as described previously (19). Substrates were applied to the EAAC1(A334E)–expressing cell through a quartz tube with an opening of about 350 µm that was positioned ~5 mm from the cell. The linear flow rate of the solutions emerging from the tube was about 5-10cm/s, resulting in typical rise times of the whole-cell current of 30-50 ms.

Ionic conditions for rapid solution exchange. To test anion-conducting properties, SCN^- was used because it enhances glutamate transporter-associated currents (5). The presence of permeating anions like SCN^- has previously been shown to permanently activate an anion current under homo-exchange conditions (6). The anion current was useful in studying this transporter because the A334E mutation interferes with steady-state glutamate transport. To investigate the glutamate concentration response relationship of the mutant transporter at steady state conditions, the pipette solution contained 500 µM glutamate, 120 mM NaSCN, 2 mM $MgCl_2$, 5 mM EGTA and 10 mM HEPES (adjusted with NaOH to pH 7.4). The extracellular solution contained varying concentrations of up to 500µM glutamate,140 mM NaMES, 2mM CaMES, 2 mM MgMES, 10mM HEPES (adjusted with NaOH to pH 7.4). These same conditions were used to test the effect of the mutation on the anion current of the transporter using voltage jump protocols as specified in the next sub-section. Nonspecific currents in the presence of 200 µM of the non-transportable competitive inhibitor TBOA (DL-*threo*-β-benzyloxyaspartic acid, (20)) were subtracted to obtain the A334E specific component.

To study the effect of the A334E mutation on the coupled transport current of the transporter, the pipette solution contained 140 mM KMES and the extracellular solution contained 500 µM glutamate, 140 mM NaMES, 2 mM $CaMES_2$, 2 mM $MgMES_2$, 10 mM HEPES, (adjusted with NaOH to pH 7.4) with and without 200 µM TBOA. To select cells with transporter mediated anion conductance, 140mM NaSCN was used in place of NaMES since the transporter activity of the mutant is almost negligible. The transporter activity was also investigated under the Na^+/Glutamate homoexchange conditions, the pipette solution contained 500µM glutamate, 140 mM NaMES, 2 mM $CaMES_2$, 2 mM $MgMES_2$ and 10 mM HEPES (adjusted with NaOH to pH 7.4) while the extracellular solution contained 500µM glutamate, 2 mM $MgMES_2$, 5 mM EGTA and 10 mM HEPES (adjusted with NaOH to pH 7.4) with and without 200µM TBOA. An extracellular solution containing 140mM NaMES in place of 140 mM NaSCN was used to test for transporter activity. The Na^+/glutamate homoexchange mode makes use of the saturation of the Na^+ and glutamate binding sites both intra- and extracellularly, making the potassium binding sites inaccessible, therefore it is not associated with steady-state transport current.

Voltage jumps. Voltage command pulses in 20 mV increments were 20 ms in duration from -100 to +80 mV from a holding potential of 0 mV. Since most cell systems contain intrinsic, voltage-sensitive channels, transporters, or pumps that lead to nonspecific transient currents, TBOA a non-transportable transporter inhibitor was used to detect specific transient currents induced by change in membrane potential (6,21).

Laser photolysis. Laser pulse photolysis experiments were performed as previously described (6). 4-Methoxy-7-nitroindolinyl (MNI)-caged glutamate (TOCRIS) was applied to the cells using a small quartz tube, and photolyzed with a light flash (355 nm Nd:YAG laser, Minilite series; Continuum, Santa Clara, CA) delivered through an optical fiber (350 µm diameter). The MNI-caged glutamate solutions were freshly prepared before starting each experiment. The yield from the photolysis of 1 mM MNI-caged glutamate was calibrated to release 200 µM free glutamate for the maximum laser energy,

according to the previously described procedure (22). Neutral density filters were applied to adjust the laser energy and attenuate glutamate release. Before and after laser-pulse photolysis experiments, a standard glutamate concentration of 100 µM was applied to the cell by solution exchange, in order to determine the concentration of glutamate released with the laser flash. After photolytic glutamate release the steady-state current amplitude was compared to the steady-state current amplitude from the calibration experiment (100 µM glutamate) and the known concentration response curve, yielding the released concentration. MNI-caged alanine was kindly provided by Dr. John Corrie and prepared as described previously (11).

L-[^{3}H] glutamate uptake. HeLa cells were cultured in Dulbecco's modified Eagle's medium supplemented with 10% fetal calf serum, 200 units/ml penicillin, 200 µg/ml streptomycin, and 2 mm glutamine. Infection with recombinant vaccinia/T7 virus vTF7-3 (23) and subsequent transfection with pBluescript KS(–) harboring EAAC-1-WT or –A334E or with the vector alone, as well as L-[^{3}H] glutamate transport, was done as published previously (24).

Data and statistical analysis. The non-linear regression fits of the experimental data were performed using the Origin (Microcal software, Northampton, MA) or Clampfit (pClamp8 software, Axon instruments, Foster City, CA). Concentration response data were described with a Michaelis-Menten-type relationship.

Experiments were performed in triplicate from at least two different cells. Error bars are given as ± standard deviation.

Electrostatic calculations. We have used the adaptive Poisson-Boltzmann solver, APBS (25), together with the APBSmem Java routines (26) to calculate the electrostatic energies of the glutamate transporter embedded into an implicit membrane in various states (HP2 open and closed, substrate bound and unbound), as described (27). In brief, the following modified version of the linearized Poisson-Boltzmann equation was used:

$$-\nabla[\varepsilon(\vec{r})\nabla\phi(\vec{r})]+\bar{\kappa}^2(\vec{r})\phi(\vec{r}) = \frac{e4\pi}{k_bT}\left(\rho(\vec{r})+\frac{\bar{\kappa}^2V}{4\pi}f(\vec{r})\right) \quad (1)$$

Here, ε is the dielectric constant, which depends on the spatial coordinate, $\phi = e\Phi/k_bT$, where Φ is the electrostatic potential, e is the elementary charge, T the temperature, and k_b the Boltzmann constant. κ is the Debye-Hückel screening constant, and ρ is the charge density. f(r) is the Heaviside step function, set to 1 in the intracellular solution and is 0 in the membrane, protein, and extracellular solution.

The total electrostatic energy, E, is then computed by summing up over the product of the local charge and the potential (28):

$$E=\int\phi(\vec{r})\rho(\vec{r})dV \quad (2)$$

where dV is the volume element. Plotting ΔE between different states versus the membrane potential yields the valence from the slope (29).

Molecular Dynamics (MD) simulations. The model system for MD simulations was set up using VMD (30), by placing an EAAT3 homology model based on the Glt_{Ph} structure (PDB code 2NWX (8), 2 Na^+ ions and, 1 aspartate bound to each subunit) into a pre-equilibrated POPC (1-palmitoyl-2-oleoylphosphatidylcholine) lipid bilayer with the dimensions 130 x 130 Å. Details can be found in (18). The total system contained 146859 atoms. The system was equilibrated for 4 ns at a constant pressure of 1 atm and a constant temperature of 310 K, using Langevin dynamics. For the following production runs, we used NVT conditions (constant volume). The cutoff for short-range interactions was 12 Å. For electrostatic interactions, we used the particle mesh Ewald method (31) implemented in NAMD. Bonds including hydrogen atoms and TIP3P water were kept rigid using SHAKE. The timestep of the simulations was 2 fs (NAMD) or 4 fs (ACEMD, (32)). All simulations were performed using the CHARMM27 force field (33).

RESULTS

Rapid glutamate application induces outward transient currents in EAAC1(A334E). The functionality of the mutant glutamate transporter was assessed by following relaxation of currents in response to rapid application of the transported substrate, glutamate. Glutamate was applied by photolysis of caged glutamate (release time constant of 200 ns (34)), providing a time resolution in the 100 μs time range. After photolytic release, glutamate binds to the transporter and the subsequent transporter reaction steps are synchronized in time, providing time-resolved information on the charge movement associated with these steps.

As shown in Fig. 1B, glutamate concentration jumps elicited outward transient current in EAAC1(A334E). This current was not observed in the presence of TBOA, a competitive glutamate transporter blocker, and in the absence of caged glutamate (Fig. 1B, bottom panel), showing that the transient current is specifically carried by the glutamate transporter. The outward current decayed with a single-exponential component with a time constant of 0.8 ± 0.02 ms at [Glu] of 100 μM. The outward transient current can be caused by either the inward movement of negative charge (Fig. 1E) and/or the outward movement of a positive charge.

In contrast, rapid glutamate application induced transient inward current in EAAC1(WT) (Fig. 1C), due to the inward movement of positive charge. It was previously suggested that this inward transient current in the wild-type transporter, which displays rising and decaying phases, is caused by the following molecular events following glutamate release (6,35-36): 1) Rapid rise of the current due to diffusion-controlled glutamate binding. 2) Bi-exponential decay of the current caused by the binding of Na^+ to the empty transporter, electrogenic glutamate translocation across the membrane, and electrogenic Na^+ binding to the glutamate-bound form of the transporter and/or a conformational change associated with this binding. All of these events cause the movement of positive charge deeper into the transmembrane electric field, until a new steady state is reached, thus generating inward transient current. A typical trace is shown in Fig. 1C and average currents are shown in Fig. 1D.

The glutamate concentration dependence of the relaxation rate constant, $1/\tau$, of the decaying phase of the current is shown in Fig. 1F, allowing insights into the molecular basis underlying the transient outward current. At low concentrations, the $1/\tau$ vs. [Glu] relationship is linear. Such a linear concentration dependence is expected for a diffusion-controlled substrate binding reaction with a bimolecular rate coefficient of $2*10^7$ $M^{-1}s^{-1}$ (Fig. 1F, dashed line), as proposed previously for EAAC1(WT) and other subtypes (35,37). However, at high [Glu], deviation from linearity is observed, with $1/\tau$ leveling off (Fig. 1F, solid line), indicating that glutamate binding is not rate limiting under these conditions. Leveling off is expected if a reaction other than binding, for example a conformational change, follows the rapid substrate binding process.

The voltage dependence of the relaxation rate constant for the rising and decaying phases of the outward transient current is shown in Fig. 1G. The rate constant associated with the decay is accelerated slightly at positive potentials, as predicted for a process in which negative charge moves into the membrane dielectric, for example glutamate binding. The weak voltage dependence of this rate constant may be caused by other, electroneutral steps partially limiting the rate of the outward current decay.

Several interpretations (Fig. 1E) are possible to explain the glutamate-induced outward current, including 1) inward movement of the negative charge of E334 (it should be noted that the pK_a value of the E334 side chain is not known, so it is also possible that the side chain is protonated and, thus, neutral), 2) inward movement of negatively-charged substrate, glutamate, and 3) inward movement of negatively-charged anions from the extracellular solution. The experiments and computational analysis described in the next paragraphs will differentiate between these possibilities.

Computational analysis suggests that glutamate binding is electrogenic. To test whether electrogenic glutamate binding (mechanism 2 in Fig. 1E) could be responsible for the observed outward charge movement in EAAC1(A334E), we performed electrostatic calculations (Figs. 2A and B) based on structural models of the open-loop, glutamate-free and closed loop, glutamate bound configurations (Fig. 2C, based on EAAC1 homology models generated using Glt_{Ph} as a template (18,27)). Solving the Poisson-Boltzmann equation allows the computation of the electrostatic energy of the two states (open loop and closed-loop/glutamate-bound), which yields the valence of the transition, when computed as a function of the membrane potential (Fig. 2A). The results (Fig. 2B) suggest that substrate binding, combined with loop closure is associated with a negative valence of -0.27 for both EAAC1(WT) and EAAC1(A334E). In contrast, loop closure alone is predicted to be associated with little charge movement (Fig. 2B) for the wild-type transporter, and a small negative valence for EAAC1(A334E). These calculations suggest that electrogenic binding of negatively charged glutamate, possibly combined with HP2 loop closure, may be the underlying mechanism for the observed outward current in Fig. 1B, with loop closure alone providing only a small contribution to charge movement.

Charge movements in response to voltage jumps. If substrate binding is electrogenic, it should be possible to perturb the binding equilibrium with step changes of the membrane potential. Consistent with this idea, transient currents were observed in EAAC1(A334E)-transfected cells in response to voltage jumps (Fig. 3). TBOA was used to isolate the EAAC1-specific component of the currents, by subtracting currents arising from other nonspecific transport activity and those arising from charging and discharging the membrane capacitance (6,21) (control, Fig. 3B). In the presence of glutamate, these currents were mainly transient in nature (Fig. 3A, the small steady state component was caused by instabilities in the cells toward the solution exchange). Integrating the off-current response yielded the charge. The charge as a function of voltage was fitted to a Boltzmann-like function (Fig. 3C). The resulting apparent valence of the A334E mutant transporter (0.67) was comparable to that of the wild-type transporter (0.64). These results suggest either that electrogenic equilibration of the glutamate translocation step still takes place (see below for more experiments that negate this possibility), or that electrogenic glutamate binding causes the voltage-induced charge movement. It should be noted that the voltage jump analysis does not provide information on the direction or the sign of the charge movement.

It has been previously shown that binding of Na^+ to the glutamate-free transporter or a conformational change linked to it can result in charge movement in the wild-type transporter (6,21). This charge movement is blocked by the non-transportable inhibitor TBOA (38). In agreement with this hypothesis, the glutamate-free transporter showed specific TBOA sensitive transient currents upon stepping the membrane potential in the presence of Na^+ (Fig. 3D). In this case, the apparent valence was 0.42 (Figs. 3F, and E, control), similar to that of the wild-type transporter. This result indicates that binding of Na^+ to the empty transporter is not altered by the A334E mutation. In fact, Na^+ binding is a prerequisite for glutamate binding (6). Therefore, based on the results showing glutamate interaction with the mutant transporter, it was not expected that Na^+ binding to the empty transporter would be affected.

Na^+-dependent leak anion currents and glutamate-induced anion currents are still functional in the A334E mutant transporter, but the activation of the anion current is slowed significantly. To test whether the A334 mutation interferes with the anion conductance of the glutamate transporter, we carried out recordings in the anion conductance mode. These experiments were performed because it is known that some mutant transporters lack transport activity, but can still support anion current (39-40). We used SCN^- as the permeating anion because the glutamate transporter-mediated anion conductance shows a high conductance for hydrophobic anions, such as

thiocyanate (5). This permeability is further enhanced by the transported substrate (5). The wild-type transporter facilitates leak anion currents in the presence of SCN^- and Na^+; this current can be inhibited by non-transportable inhibitors, such as TBOA (35,41). Fig. 4A shows that Na^+-induced leak anion currents are also present in EAAC1(A334E). These currents are directed inward, due to outflow of internal SCN^- through the Na^+-induced leak anion conductance, which can be inhibited by TBOA.

In the presence of substrate, Na^+ and a permeable anion, glutamate transporters facilitate what is referred to as a glutamate-gated anion conductance. Glutamate has to bind to the transporter for its activation, but the conductance is not thermodynamically coupled to glutamate transport. This anion current strictly follows the driving force for anions (5,35). Results shown in Fig. 4B illustrate that EAAC1(A334E) exhibits a glutamate-gated anion conductance in the homo-exchange mode (glutamate was present on both sides of the cell membrane). In the presence of intracellular thiocyanate, the anion current was inward directed, and its magnitude increased in the presence of glutamate as supported by previous studies on the wild-type transporter (5). The voltage dependence of this anion current (shown in Figs. 4C and D) is comparable to that observed previously in the wild-type transporter (42). Subtraction of current in the presence of TBOA was used to isolate the specific current (Figs. 4A and B). EAAC1(A334E) also exhibited anion currents with SCN^- in the extracellular rather than in the intra-cellular medium. Now an outward current that was sensitive to TBOA was generated (not shown), consistent with uncoupled anion flow into the cell. Together, these results indicate that the A334E mutation does not substantially inhibit the anion conductance of the transporter.

The glutamate transporter anion conductance can be activated by application of glutamate. In the wild-type transporter, the anion conductance is activated by glutamate with a time constant of 0.9 ± 0.15 ms (Fig. 4F, grey trace). In contrast, the activation of the anion conductance by glutamate is dramatically slowed in EAAC1(A334E), with a time constant, τ, of 1000 ± 200 ms (Fig. 4E, black trace, WT control is shown for comparison in grey), indicating a 1000-fold slower activation of the anion conductance than in the wild-type transporter. Fig. 4F shows the activation of the EAAC1(A334E) anion current (black trace) with high time resolution (millisecond time scale), demonstrating little activation within the first 60 milliseconds after glutamate release, in contrast to the wild-type transporter (grey). The time course of the activation of the anion conductance by glutamate is thought to reflect the glutamate-induced increase of the population of the intermediate occluded state (43-44) along the translocation pathway, suggesting that the rate of formation of this state is severely inhibited by the A334E mutation.

The apparent affinity for glutamate is not significantly affected by the A334E mutation. Fig. 5A shows a typical current recording from the A334E mutant transporter when glutamate was applied by rapid solution exchange in the Na^+/glutamate homo-exchange mode. The intracellular solution contained SCN^- and the inward directed currents are arising from the anion's exit from the cell (V = 0 mV). The amplitude of the anion current was dependent on the glutamate concentration in a Michaelis-Menten-like fashion (Fig. 5B). The apparent affinity (K_m) for glutamate was determined to be 30 ± 5μM, while that of the wild type transporter was 19 ± 8 μM. These results show that the mutation did not dramatically alter the apparent affinity of the transporter for the substrate. Therefore, the dramatic changes in functional behavior of the mutant transporter are not caused by changes in the substrate binding pocket.

Coupled steady-state transport current is not observed in the A334E mutant transporter. Wild-type glutamate transporters catalyze significant voltage-dependent inward transport current, caused by the inward movement of two positive charges (4) for each transported glutamate anion (Fig. 6B). In contrast, EAAC1(A334E)-expressing cells displayed little, if any, transport current when glutamate was applied to the extracellular side in the presence of internal K^+

(Fig. 6A, forward transport conditions, glutamate was applied as indicated by the grey bar and removed at t = 4s) at 0 mV, as well as at increased driving force (up to -100 mV, Fig. 6B). In addition, [^{3}H] glutamate uptake is strongly inhibited by the mutation (Fig. 6C). Together, these results suggest that glutamate translocation and/or K^+-induced relocation is/are slowed.

Poisson-Boltzmann analysis of the membrane potential distribution along the membrane normal for an EAAC1 homology model, based on Glt_{Ph}, suggests that the 334 side chain moves through a major proportion of the transmembrane electric field during the outward- to inward-facing transition (Figs. 6D and E, position of A334E indicated by arrows, membrane potential color coded from 0 mV (blue) to -100 mV (red)). While the valence associated with this transition is positive for the wild type transporter (18), as determined from experiment, as well as computation, z = +0.15, Fig. 6F), the computed valence for the mutant transporter is large and negative (z = -0.71, Fig. 6F, if the 334E side chain is deprotonated), implying that the large alteration of the electrostatic balance of the translocation process is likely to inhibit both the translocation and the K^+-induced relocation reactions.

Molecular dynamics simulations of wild-type and mutant transporter. To test the effects of the A334E mutation *in-silico*, we performed 1 μs molecular dynamics (MD) simulations (Fig. 7). The structures at the endpoint of the simulations for wild-type and mutant EAAC1 are shown in Fig. 7A and B. The mutant transporter showed significant distortion of the structure at the tip of HP1 (Figs. 7A and B), while the substrate binding site and HP2 structures were virtually unchanged (not shown). Consistent with these findings, the substrate was stable in the EAAC1(A334E) and wild-type binding sites for several 100 ns up to 1 μs (Figs. 7C and D), consistent with the experimental data showing little effect of the mutant on substrate apparent affinity. To quantify the effect of the A334E mutation on the structure at the tip of HP1, we determined the radial distribution function of the distance of water from the Cβ atom of A334 and A334E (Figs. 7E and F). The results show that water penetration to the tip of HP1 is significantly increased in the mutant transporter, possibly caused by the introduction of a potential negative charge in this position. This structural distortion could explain the inability of the transporter to catalyze translocation, while preserving the ability to bind the substrate.

Sodium ions in site Na1 and the predicted Na3' site were stable in all simulations performed and did not dissociate within 1 μs (data not shown). These results are consistent with the voltage jump analysis, indicating that the A334E mutation does not interfere with Na^+ binding to the empty transporter. However, sodium ions were unstable in simulations of the Na2 site of the mutant transporter, dissociating within nanoseconds of the start of the simulation. Because binding of sodium to the Na2 site is thought to be required for the closure of the HP2 loop (8), it is possible that defective Na^+ binding to the loaded transporter is the reason for the inability of the transporter to catalyze glutamate translocation.

Sodium dependence of the transient outward current. Upon close inspection, the transient outward current observed after rapid glutamate application to EAAC1(A334E) is followed by a minor, but significant inward component (Fig. 8A). This result raises the possibility that some electrogenic reactions, such as Na^+ binding to the empty transporter, may still be functional after mutation, as indicated by our results shown above. To test this hypothesis, we repeated the [glutamate] jump experiment at lower extracellular [Na^+] (20 mM, Fig. 8A), shifting the Na^+ binding equilibrium further to the non-bound state. Interestingly, most (but not all, Fig. 8B) of the outward charge movement was eliminated, but a sizable inward current was observed. This current decayed significantly slower than the outward current at 140 mM Na^+ (Fig. 8C). These results suggest that electrogenic Na^+ rebinding to the empty transporter, which is still functional in EAAC1(A334E) (Fig. 3), starts masking the glutamate-induced outward charge movement at low sodium concentrations.

Binding of a neutral (zwitterionic) substrate does not induce outward charge movement. A glutamate transporter with the mutation R446Q was shown previously to bind neutral amino acids, such as glutamine and alanine, instead of the negatively charge glutamate. We exploited this mutation to test whether neutralizing the substrate would eliminate the outward charge movement. The results of rapid alanine application to the EAAC1(R446Q,A334E) double mutant transporter are shown in Fig. 9. Rapid alanine application (300 μM) by photolysis of caged alanine resulted in a transient inward current (Fig. 9A), in contrast to the outward current observed upon glutamate application to EAAC1(A334E). This alanine concentration is close to saturating, as demonstrated by the concentration response curve shown in Fig. 9B. These results demonstrate that a negatively-charged substrate is necessary to generate transient outward current. They also suggest that the outward current is not caused by inward movement of the Glu-334 side chain in the mutant transporter, which is preserved in the double-mutant transporter.

DISCUSSION

The major finding of this study is that binding of negatively-charged substrate to the glutamate transporter EAAC1, or a conformational change closely associated with binding, is/are electrogenic, and, thus associated with apparent outward charge movement, caused by inward movement of a negative charge (Figs. 1B, 2, 6A). This charge movement was uncovered in experiments with a transporter with an Ala to Glu mutation in position 334, located at the tip of hairpin loop 1. The results suggest that the outward charge movement is hidden in the wild-type transporter, because it is overcompensated by simultaneous inward movement of positive charge from glutamate translocation, and Na^+ binding to the empty and substrate-bound transporter. This is an important finding because glutamate binding adds to the substantial list of electrogenic partial reactions in glutamate transporters (6,27,45), in which charge movement within the membrane is distributed over several reaction steps. This includes Na^+ binding, dissociation, K^+-induced relocation, and substrate translocation steps (27,46).

Based on the current knowledge of the alternating access, elevator-like transport model of glutamate transporters (47-48), the existence of an electrogenic substrate binding process is not unexpected. In current models, substrate binds to the open-loop configuration, in which HP2 is open to the extracellular side (49-50). Upon binding, closure of HP2 can occur, generating a complex that can undergo the structural changes associated with the translocation reaction. Glutamate, in this occluded complex, is buried more deeply within the membrane, thus generating charge movement. Our electrostatic calculations (Fig. 2) suggest that the binding process occurs within part of the transmembrane electric field, while the HP2 closure process is associated with little, if any, voltage dependence.

We performed kinetic simulations to provide a quantitative explanation of the experimental results. The simulations are based on a sequential Na^+-substrate-Na^+ binding model (Fig. 10), which has been proposed in previous work (6,51-52). We have also included a reaction step following substrate binding, possible a conformational change, evidence for which has been obtained in (6,40). The insets shown in Fig. 10 illustrate that such a model can reproduce the experimental data (Fig. 1) well, when assuming that Na^+ binding to the glutamate-bound transporter and translocation is inhibited by the A334E mutation, while the kinetics of Na^+ binding to the empty transporter and glutamate binding remain unchanged. Inward movement of negative charge (valence = -0.16) was modeled into the glutamate binding step. The detailed kinetic parameters, which were not fitted but rather estimated based on the present and previous work are listen in the legend of Fig. 10. It cannot be excluded that other sets of parameters can also account for the experimental data, including negative valence modeled for the step following the actual glutamate binding.

The voltage dependence of the apparent affinity of the wild-type transporter for glutamate has been investigated previously at steady state

(52). At 100 mM [Na^+], this affinity was found to be only weakly dependent on the membrane potential, slightly increasing at positive voltages. While increased affinity at positive potentials is expected for voltage-dependent glutamate binding, many processes other than glutamate binding affect the experimentally-determined apparent affinity at steady state. Most likely, the apparent affinity is mainly controlled by the two slowest steps in the cycle, the voltage-dependent glutamate translocation process, as well as the K^+-dependent relocation step (see (35) for equations). Since both of those processes are accelerated in an almost equal fashion by more negative trans-membrane potential, the apparent affinity is relatively unchanged at different voltages. These results further demonstrate that it can be difficult to obtain information on the voltage dependence of non-rate limiting partial reactions at steady state, but that time resolved, pre-steady-state analysis is necessary to detect electrogenicity, as has been shown for other transporters (53).

Our results allow us to clearly distinguish between the proposed electrogenic substrate binding model and two alternative major mechanisms that could explain the outward charge movement observed in the mutant transporter. The charge movement cannot be caused by chloride (mechanism 3 in Fig. 1E, 3) as a charge-carrying species, because it is still present in the absence of chloride in both the intracellular and extracellular solutions (Fig. 1). Interestingly, the A334E mutation does not interfere with the ability of the transporter to support the anion conductance (Fig. 4). This result is somewhat surprising because the side chain of A334 is very close to the residues at the tip of HP1, which have been recently proposed to contribute to anion pore formation (54). It would be expected that an additional negative charge close to those positions would electrostatically inhibit anions from entering the pore. However, our MD simulations suggest that water permeation is increased at the tip of HP1 by the mutation. This effect, possibly enhancing anion permeation, may counteract any negative effects of electrostatics.

The activation of the anion conductance is dramatically slowed in the A334E mutant transporter relative to the wild-type. It was proposed that the anion conducting state corresponds to the intermediate, occluded state observed in a crystal structure (43-44,54-56). If this is the case, transition from the outward-occluded state to the intermediate state is slowed by the A334E mutation, consistent with our observation of lack of steady state transport (Fig. 6). It is interesting to speculate on the structural basis of the defective step of the A334E mutation. In the wild-type transporter, the closure of the external gate/HP2 loop, requires the binding of the "last" sodium to the Na2 site (8) and this is followed by the translocation step thought to occur via an "elevator-like" movement (47-48). Even in the absence of glutamate, sodium can activate the anion conductance. This suggests that the intermediate anion conducting state (54-55), which requires a partial "elevator" movement of the transport domain, can be reached in the presence of sodium alone. Thus it is possible, that if A334E transporters are defective in the binding of the last sodium to the Na2 site, a partial "elevator" movement through the membrane electric field still can take place which reflects the electrogenic glutamate binding step. Evidently, such a scenario also accounts for the defective transport by the mutant (Fig. 6).

Our results are somewhat reminiscent of what has been observed in a transporter with another charge-altering mutation, D439N (40), which also showed a dramatic slowdown of anion current activation by glutamate. However, in the D439N mutation a potential negative charge is eliminated, not introduced, as opposed to the A334E mutant transporter. Rapid application of glutamate induces transient outward current in EAAC1(D439N) (not shown), that displays similar kinetics of the one observed in the A334E mutant transporter. Therefore, the molecular basis of the effect of the two oppositely charge-altering mutations, namely the slowing of the Na^+-dependent processes of the glutamate-bound transporter, is most likely the same.

The second alternative mechanism is based on inward movement of negative charge in position 334 (Mechanism 1 in Fig. 1E). However, in the double mutant transporter A334E-R446Q, which binds neutral instead of acidic amino acids, no outward charge movement is observed (Fig. 9). Instead, inward transient current is observed, which is caused by the inward movement of bound Na^+, as in the wild-type transporter and glutamate as substrate. If the transient outward current was caused by inward movement of A334E, it should still be observed in the double mutant transporter. These results directly show that the outward charge movement is not caused by inward movement of the A334E side chain.

Our results indicate that glutamate translocation is impaired by the A334E mutation. In light of the elevator type mechanism for transport, in which the tip of HP1 moves through a large part of the hydrophobic interior of the membrane (see electrostatic calculations in Fig. 6), this result is not surprising. The glutamate side chain in position 334 may add negative charge, or at least hydrophilic character to the tip of HP1, raising the possibility that the energy barrier for motion of HP1 across the bilayer is increased.

Is glutamate binding from the intracellular side of the membrane also electrogenic? At present, our data do not provide insights into this question. However, considering the symmetrical nature of the transporter structure, and the known electrogenic binding of Na^+ to its intracellular binding site (46), it is likely that intracellular glutamate binding is also electrogenic. This possibility could be tested by rapidly applying glutamate to the intracellular side of the membrane, which we have done in the past in the wild-type transporter (46). Such experiments with the A334E mutant transporter will be performed in the future.

The tip of HP1 has been investigated in previous mutagenesis studies and has been found to be important for substrate interaction, as well as K^+-induced relocation of the transporter (57). In addition, our results suggest that this region may be also involved in controlling reactions associated with the translocation process.

Glutamate transporters are known to regulate the glutamate concentration in the synaptic cleft after pre-synaptic release. Due to the relatively slow, millisecond kinetics of glutamate translocation across the membrane, it was hypothesized that rapid buffering of glutamate through binding to the transporter binding site contributes to controlling the synaptic glutamate concentration at short times after release (58). Buffering is possible due to the large density of transporter binding sites in and around the synaptic contacts, which was estimated to about 10,000 per μm^2 (1). Buffering kinetics were incorporated into simulations of the time dependence of synaptic glutamate concentration (2,59). Interestingly, one of these studies showed a time dependence of the K_d of the transporter for glutamate, which decreases over time (2). Thus, buffering occurs with a K_d of 100 μM directly after release, decreasing to a K_d of 5 μM at steady state. This suggests that the buffered glutamate concentration also decreases at increasing times after release. The finding of voltage dependent glutamate binding adds another variable, suggesting that the K_d for buffering not only depends on time, but also on membrane potential. Thus, the optimum buffering range would be shifted to lower concentrations at depolarized membrane potential. This effect could be particularly important for neuronal glutamate transporters, such as EAAC1, due to the voltage changes in neuronal membranes during synaptic transmission events.

Conclusions. In summary, we have demonstrated that binding of the anionic organic substrate to the neuronal glutamate transporter EAAC1 is electrogenic, and, thus, associated with transient outward charge movement when glutamate binds from the extracellular side of the membrane. This finding is important because it further supports previous evidence on the distribution of voltage dependent partial reactions over the transport cycle, resulting in a relatively weak voltage dependence of steady-state glutamate transport. The results also suggest that

voltage dependence of the K_d for glutamate should be included in future simulations of the time dependence of synaptic [glutamate] after pre-synaptic release. Our findings may provide insight into substrate binding by other secondary-active transporters, in which charged organic or inorganic substrates are transported across membranes.

ACKNOWLEDGEMENTS

This work was supported by by the National Science Foundation Grant 1515028 awarded to CG and a Binational Science Foundation (BSF), Grant 2007051 awarded to CG and BIK. We thank Dr. John E. Corrie for kindly providing caged alanine.

CONFLICT OF INTEREST

The authors declare that they have no conflicts of interest with the contents of this article.

AUTHOR CONTRIBUTIONS

Rose Tanui: Experimentation, design, analysis and interpretation of data, writing of manuscript
Zhen Tao: Experimentation and data analysis
Nechama Silverstein: Experimentation and data analysis
Baruch Kanner: Data analysis, interpretation and writing of manuscript
Christof Grewer: Experimentation, design, analysis and interpretation of data, writing of manuscript

REFERENCES

1. Danbolt, N. C. (2001) Glutamate uptake. *Prog Neurobiol* **65**, 1-105
2. Grewer, C., Gameiro, A., Zhang, Z., Tao, Z., Braams, S., and Rauen, T. (2008) Glutamate forward and reverse transport: from molecular mechanism to transporter-mediated release after ischemia. *IUBMB Life* **60**, 609-619
3. Levy, L. M., Warr, O., and Attwell, D. (1998) Stoichiometry of the glial glutamate transporter GLT-1 expressed inducibly in a Chinese hamster ovary cell line selected for low endogenous Na+-dependent glutamate uptake. *J Neurosci* **18**, 9620-9628
4. Zerangue, N., and Kavanaugh, M. P. (1996) Flux coupling in a neuronal glutamate transporter. *Nature* **383**, 634-637
5. Wadiche, J. I., Amara, S. G., and Kavanaugh, M. P. (1995) Ion fluxes associated with excitatory amino acid transport. *Neuron* **15**, 721-728
6. Watzke, N., Bamberg, E., and Grewer, C. (2001) Early intermediates in the transport cycle of the neuronal excitatory amino acid carrier EAAC1. *Journal of General Physiology* **117**, 547-562
7. Bastug, T., Heinzelmann, G., Kuyucak, S., Salim, M., Vandenberg, R. J., and Ryan, R. M. (2012) Position of the third Na+ site in the aspartate transporter GltPh and the human glutamate transporter, EAAT1. *PLoS One* **7**, e33058
8. Boudker, O., Ryan, R. M., Yernool, D., Shimamoto, K., and Gouaux, E. (2007) Coupling substrate and ion binding to extracellular gate of a sodium-dependent aspartate transporter. *Nature* **445**, 387-393
9. Loo, D. D., Hazama, A., Supplisson, S., Turk, E., and Wright, E. M. (1993) Relaxation kinetics of the Na+/glucose cotransporter. *Proc Natl Acad Sci U S A* **90**, 5767-5771
10. Lu, C. C., and Hilgemann, D. W. (1999) GAT1 (GABA : Na+: Cl-) cotransport function - Kinetic studies in giant Xenopus oocyte membrane patches. *Journal of General Physiology* **114**, 445-457
11. Zhang, Z., Papageorgiou, G., Corrie, J. E., and Grewer, C. (2007) Pre-steady-state currents in neutral amino acid transporters induced by photolysis of a new caged alanine derivative. *Biochemistry* **46**, 3872-3880
12. Forster, I. C., Kohler, K., Biber, J., and Murer, H. (2002) Forging the link between structure and function of electrogenic cotransporters: the renal type IIa Na+/Pi cotransporter as a case study. *Prog Biophys Mol Biol* **80**, 69-108
13. Watzke, N., Rauen, T., Bamberg, E., and Grewer, C. (2000) On the mechanism of proton transport by the neuronal excitatory amino acid carrier 1. *J Gen Physiol* **116**, 609-622
14. Zerangue, N., and Kavanaugh, M. P. (1996) Interaction of L-cysteine with a human excitatory amino acid transporter. *Journal of Physiology* **493**, 419-423
15. Bendahan, A., Armon, A., Madani, N., Kavanaugh, M. P., and Kanner, B. I. (2000) Arginine 447 plays a pivotal role in substrate interactions in a neuronal glutamate transporter. *Journal of Biological Chemistry* **275**, 37436-37442
16. Yernool, D., Boudker, O., Jin, Y., and Gouaux, E. (2004) Structure of a glutamate transporter homologue from Pyrococcus horikoshii. *Nature* **431**, 811-818
17. Hamill, O. P., Marty, A., Neher, E., Sakmann, B., and Sigworth, F. J. (1981) Improved patch-clamp techniques for high-resolution current recording from cells and cell-free membrane patches. *Pflugers Arch* **391**, 85-100
18. Mwaura, J., Tao, Z., James, H., Albers, T., Schwartz, A., and Grewer, C. (2012) Protonation state of a conserved acidic amino acid involved in Na(+) binding to the glutamate transporter EAAC1. *ACS Chem Neurosci* **3**, 1073-1083

19. Grewer, C. (1999) Investigation of the alpha(1)-glycine receptor channel-opening kinetics in the submillisecond time domain. *Biophys J* **77**, 727-738
20. Shimamoto, K., Lebrun, B., Yasuda-Kamatani, Y., Sakaitani, M., Shigeri, Y., Yumoto, N., and Nakajima, T. (1998) DL-threo-beta-benzyloxyaspartate, a potent blocker of excitatory amino acid transporters. *Mol Pharmacol* **53**, 195-201
21. Wadiche, J. I., Arriza, J. L., Amara, S. G., and Kavanaugh, M. P. (1995) Kinetics of a Human Glutamate Transporter. *Neuron* **14**, 1019-1027
22. Grewer, C., Jager, J., Carpenter, B. K., and Hess, G. P. (2000) A new photolabile precursor of glycine with improved properties: A tool for chemical kinetic investigations of the glycine receptor. *Biochemistry* **39**, 2063-2070
23. Fuerst, T. R., Niles, E. G., Studier, F. W., and Moss, B. (1986) Eukaryotic transient-expression system based on recombinant vaccinia virus that synthesizes bacteriophage T7 RNA polymerase. *Proc Natl Acad Sci U S A* **83**, 8122-8126
24. Pines, G., Zhang, Y., and Kanner, B. I. (1995) Glutamate 404 is involved in the substrate discrimination of GLT-1, a (Na+ + K+)-coupled glutamate transporter from rat brain. *J Biol Chem* **270**, 17093-17097
25. Baker, N. A., Sept, D., Joseph, S., Holst, M. J., and McCammon, J. A. (2001) Electrostatics of nanosystems: application to microtubules and the ribosome. *Proc Natl Acad Sci U S A* **98**, 10037-10041
26. Callenberg, K. M., Choudhary, O. P., de Forest, G. L., Gohara, D. W., Baker, N. A., and Grabe, M. (2010) APBSmem: a graphical interface for electrostatic calculations at the membrane. *PLoS One* **5**
27. Grewer, C., Zhang, Z., Mwaura, J., Albers, T., Schwartz, A., and Gameiro, A. (2012) Charge compensation mechanism of a Na+-coupled, secondary active glutamate transporter. *J Biol Chem* **287**, 26921-26931
28. Silva, J. R., Pan, H., Wu, D., Nekouzadeh, A., Decker, K. F., Cui, J., Baker, N. A., Sept, D., and Rudy, Y. (2009) A multiscale model linking ion-channel molecular dynamics and electrostatics to the cardiac action potential. *Proc Natl Acad Sci U S A* **106**, 11102-11106
29. Choudhary, O. P., Ujwal, R., Kowallis, W., Coalson, R., Abramson, J., and Grabe, M. (2010) The electrostatics of VDAC: implications for selectivity and gating. *J Mol Biol* **396**, 580-592
30. Humphrey, W., Dalke, A., and Schulten, K. (1996) VMD: visual molecular dynamics. *J Mol Graph* **14**, 33-38, 27-38
31. Darden, T., York, D. M., and Pdersen, L. (1993) Particle mesh Ewald: An N log(N) method for Ewald sums in large systems. *J. Chem. Phys.* **98**, 10089-10092
32. Harvey, M. J., Giupponi, G., and Fabritiis, G. D. (2009) ACEMD: Accelerating Biomolecular Dynamics in the Microsecond Time Scale. *J Chem Theory Comput* **5**, 1632-1639
33. MacKerell, A. D., Bashford, D., Bellott, Dunbrack, R. L., Evanseck, J. D., Field, M. J., Fischer, S., Gao, J., Guo, H., Ha, S., Joseph-McCarthy, D., Kuchnir, L., Kuczera, K., Lau, F. T. K., Mattos, C., Michnick, S., Ngo, T., Nguyen, D. T., Prodhom, B., Reiher, W. E., Roux, B., Schlenkrich, M., Smith, J. C., Stote, R., Straub, J., Watanabe, M., Wiórkiewicz-Kuczera, J., Yin, D., and Karplus, M. (1998) All-Atom Empirical Potential for Molecular Modeling and Dynamics Studies of Proteins†. *The Journal of Physical Chemistry B* **102**, 3586-3616
34. Maier, W., Corrie, J. E., Papageorgiou, G., Laube, B., and Grewer, C. (2005) Comparative analysis of inhibitory effects of caged ligands for the NMDA receptor. *J Neurosci Methods* **142**, 1-9
35. Grewer, C., Watzke, N., Wiessner, M., and Rauen, T. (2000) Glutamate translocation of the neuronal glutamate transporter EAAC1 occurs within milliseconds. *Proceedings of the National Academy of Sciences of the United States of America* **97**, 9706-9711
36. Otis, T. S., and Kavanaugh, M. P. (2000) Isolation of current components and partial reaction cycles in the glial glutamate transporter EAAT2. *J Neurosci* **20**, 2749-2757

37. Wadiche, J. I., and Kavanaugh, M. P. (1998) Macroscopic and microscopic properties of a cloned glutamate transporter/chloride channel. *J Neurosci* **18**, 7650-7661
38. Mim, C., Tao, Z., and Grewer, C. (2007) Two conformational changes are associated with glutamate translocation by the glutamate transporter EAAC1. *Biochemistry* **46**, 9007-9018
39. Seal, R. P., Shigeri, Y., Eliasof, S., Leighton, B. H., and Amara, S. G. (2001) Sulfhydryl modification of V449C in the glutamate transporter EAAT1 abolishes substrate transport but not the substrate-gated anion conductance. *Proceedings of the National Academy of Sciences of the United States of America* **98**, 15324-15329
40. Tao, Z., and Grewer, C. (2007) Cooperation of the conserved aspartate 439 and bound amino acid substrate is important for high-affinity Na+ binding to the glutamate transporter EAAC1. *J Gen Physiol* **129**, 331-344
41. Watzke, N., and Grewer, C. (2001) The anion conductance of the glutamate transporter EAAC1 depends on the direction of glutamate transport. *FEBS Lett* **503**, 121-125
42. Tao, Z., Zhang, Z., and Grewer, C. (2006) Neutralization of the aspartic acid residue Asp-367, but not Asp-454, inhibits binding of Na+ to the glutamate-free form and cycling of the glutamate transporter EAAC1. *Journal of Biological Chemistry* **281**, 10263-10272
43. Cater, R. J., Vandenberg, R. J., and Ryan, R. M. (2014) The domain interface of the human glutamate transporter EAAT1 mediates chloride permeation. *Biophys J* **107**, 621-629
44. Grewer, C., and Gameiro, A. (2014) How do glutamate transporters function as transporters and ion channels? *Biophys J* **107**, 546-547
45. Bergles, D. E., Tzingounis, A. V., and Jahr, C. E. (2002) Comparison of coupled and uncoupled currents during glutamate uptake by GLT-1 transporters. *J Neurosci* **22**, 10153-10162
46. Zhang, Z., Tao, Z., Gameiro, A., Barcelona, S., Braams, S., Rauen, T., and Grewer, C. (2007) Transport direction determines the kinetics of substrate transport by the glutamate transporter EAAC1. *Proc Natl Acad Sci U S A* **104**, 18025-18030
47. Reyes, N., Ginter, C., and Boudker, O. (2009) Transport mechanism of a bacterial homologue of glutamate transporters. *Nature* **462**, 880-885
48. Crisman, T. J., Qu, S., Kanner, B. I., and Forrest, L. R. (2009) Inward-facing conformation of glutamate transporters as revealed by their inverted-topology structural repeats. *Proc Natl Acad Sci U S A* **106**, 20752-20757
49. Huang, Z., and Tajkhorshid, E. (2008) Dynamics of the extracellular gate and ion-substrate coupling in the glutamate transporter. *Biophys J* **95**, 2292-2300
50. Shrivastava, I. H., Jiang, J., Amara, S. G., and Bahar, I. (2008) Time-resolved mechanism of extracellular gate opening and substrate binding in a glutamate transporter. *J Biol Chem* **283**, 28680-28690
51. Kanai, Y., and Hediger, M. A. (1992) Primary Structure and Functional Characterization of a High-Affinity Glutamate Transporter. *Nature* **360**, 467-471
52. Kanai, Y., Nussberger, S., Romero, M. F., Boron, W. F., Hebert, S. C., and Hediger, M. A. (1995) Electrogenic Properties of the Epithelial and Neuronal High-Affinity Glutamate Transporter. *Journal of Biological Chemistry* **270**, 16561-16568
53. Li, Y., Hasenhuetl, P. S., Schicker, K., Sitte, H. H., Freissmuth, M., and Sandtner, W. (2015) Dual Action of Zn2+ on the Transport Cycle of the Dopamine Transporter. *J Biol Chem* **290**, 31069-31076
54. Machtens, J. P., Kortzak, D., Lansche, C., Leinenweber, A., Kilian, P., Begemann, B., Zachariae, U., Ewers, D., de Groot, B. L., Briones, R., and Fahlke, C. (2015) Mechanisms of anion conduction by coupled glutamate transporters. *Cell* **160**, 542-553
55. Verdon, G., and Boudker, O. (2012) Crystal structure of an asymmetric trimer of a bacterial glutamate transporter homolog. *Nat Struct Mol Biol* **19**, 355-357

56. Shabaneh, M., Rosental, N., and Kanner, B. I. (2014) Disulfide cross-linking of transport and trimerization domains of a neuronal glutamate transporter restricts the role of the substrate to the gating of the anion conductance. *J Biol Chem* **289**, 11175-11182
57. Ryan, R. M., Kortt, N. C., Sirivanta, T., and Vandenberg, R. J. (2010) The position of an arginine residue influences substrate affinity and K+ coupling in the human glutamate transporter, EAAT1. *J Neurochem* **114**, 565-575
58. Diamond, J. S., and Jahr, C. E. (1997) Transporters buffer synaptically released glutamate on a submillisecond time scale. *J Neurosci* **17**, 4672-4687
59. Holmes, W. R. (1995) Modeling the effect of glutamate diffusion and uptake on NMDA and non-NMDA receptor saturation. *Biophys J* **69**, 1734-1747
60. Mim, C., Balani, P., Rauen, T., and Grewer, C. (2005) The glutamate transporter subtypes EAAT4 and EAATs 1-3 transport glutamate with dramatically different kinetics and voltage dependence but share a common uptake mechanism. *Journal of General Physiology* **126**, 571-589

ABBREVIATIONS

EAAC1 -Excitatory amino acid carrier 1
EGTA-ethylene glycol-bis-(beta-aminoethyl ether)-N,N,N',N'-tetraacetic acid
SCN^--thiocyanate anion
TBOA-DL-threo-β-benzyloxyaspartic acid
MNI- methoxynitroindoline
HP-hairpin loop
Glu-glutamate
SLC-solute carrier
POPC- 1-palmitoyl-2-oleoylphosphatidylcholine
NVT-constant number of particles, volume and temperature (canonical ensemble)

FIGURE LEGENDS

Figure 1: Glutamate-induced outward charge movement in the transporter with the A334E mutation under forward transport conditions. (A) Conserved serine-rich motif in hairpin loop 1 (HL1), which harbors the A334 to E mutation. **(B)** Typical transient outward current (A334E) in response to glutamate application through photolysis of 1 mM MNI-caged glutamate at time t = 0. Controls (lower panel) show the absence of a response in the presence of the EAAC1 inhibitor TBOA, and in the absence of caged glutamate. The dotted line represents 0 current, illustrating the slight inward current at longer times. **(C)** Inward current response in the WT transporter to glutamate under the same conditions as in (C). **(D)** Average peak currents in EAAC1(A334E) and EAAC(WT). All recordings were performed at V = 0 mV under forward transport conditions with 140 mM NaMES (external) and 140 mM KMES (internal). No anion current was observed due to the absence of permeable anions. **(E)** Potential mechanistic explanations for the outward current response. **(F)** Relaxation rate constant of the decaying phase of the glutamate-induced outward current as a function of [glutamate]. The dashed line represents the expected behavior for diffusion-controlled binding with a bimolecular rate constant of 2×10^7 $M^{-1}s^{-1}$. **(G)** Relaxation rate constants for the rising (▲) and decaying phase (●) of the EAAC1(A334E) glutamate-induced transient outward current as a function of the voltage. The rate constants, $1/\tau$, were obtained from fitting a two-exponential function to the experimental data, with a typical trace at 0 mV shown in (B).

Figure 2: Poisson Boltzmann analysis predicts electrogenic substrate binding/loop closure. (A) Calculation of the energy differences between the open-loop state and the closed-loop state with and without substrate present, as a function of the transmembrane potential. The slope of the lines is representative of the valence of the process. Symbols (■) and (○) are superimposed. **(B)** Computed valences for the processes in A334E and WT transporters. **(C)** Illustration of the structural HP2 loop-closure rearrangement used for the computations in (A) and (B).

Figure 3: Transient EAAC1(A334E) currents induced by voltage jumps show charge movement in the absence and presence of glutamate. (A) Transient currents elicited by voltage jumps from 0 mV to a range of voltages from -100 to +80 mV in the presence of glutamate under Na^+/glutamate homo-exchange conditions (Na^+/glutamate on both sides of the membrane, see inset in (C)). **(B)** A control trace obtained from the same cell in (A) when two separate I(glu +TBOA) recordings are subtracted from one another, showing stability of the cell. The inset shows original, non-subtracted traces at -100 mV. **(D)** Transient currents elicited by voltage jumps as in (A) in the presence of Na^+ and the absence of the glutamate. **(E)** Control currents obtained by subtracting two separate I(Na^+ +TBOA) recordings from one another. The inset shows original, non-subtracted traces at -100 mV. **(C and F)** Voltage dependence of the charge elicited (C) in the glutamate-bound transporter and (F) in the glutamate-free transporter. The charge (Q_{off}) was obtained by the integration of the transient currents of the off response from the A334E mutant transporter. The red lines represent fits to the Boltzmann equation with an apparent valence of 0.67 and a midpoint potential of -34.0 mV for the glutamate-bound transporter and an apparent valence of 0.42 and a midpoint potential of -37.8 mV for the glutamate-free transporter. The intracellular solution contained 140 mM NaMES and 10 mM glutamate, the extracellular solution 140 mM NaMES with (A, B) and without (C, D) 10 mM glutamate.

Figure 4: Sodium- and glutamate-induced anion conductances of the glutamate transporter are functional the A334E mutant transporter, but activation by glutamate is slowed. (A) Shows a typical current recording in response to voltage jumps (from -100 to + 80 mV in increments of 20 mV for a duration of 20 ms) from a cell in the presence of 140 mM intracellular SCN^-. Na^+ was applied extracellularly in the absence of glutamate. Non-subtracted traces at -100 mV are shown in the top inset. **(B)** Recording as in (A), but in the presence of glutamate. **(C and D)** represent the I-V relationships obtained from responses shown in (A and B). All currents are inwardly directed due to the outflow of

SCN^- from the cell. All unspecific currents were subtracted using TBOA. For (A-D), the intracellular solution contained 140 mM NaSCN and 0.5 mM glutamate (homoexchange). **(E)** Slow rise of EAAC11(A334E) anion current (black trace) induced by rapid application of 100 μM glutamate (indicated by the grey bar), in comparison to fast rise of EAAC1(WT) current (grey trace). **(F)** Experiment similar as in (E), but glutamate application was through photolysis of 1 mM MNI-caged glutamate at time 0 (indicated by the arrow). The rapid outward transient current in EAAC1(A334E) (black trace), which is the same as in the transport mode, is followed by slow activation of inward anion currents caused by anion outflow. The grey trace shows the WT control. For E and F, the intracellular solution contained 140 mM KSCN, and the extracellular solution 140 mM NaMES.

Figure 5: The apparent affinity for glutamate is not significantly altered by the A3334E mutation. **(A)** Typical whole-cell current recording upon application of 100 μM glutamate through rapid solution exchange to EAAC1(A334E) at a holding potential of 0 mV. The recordings were performed in the homoexchange mode (140 mM Na^+ and 10 mM glutamate on both sides of the membrane, see inset) with intracellular SCN^- and extracellular MES^- as anions. **(B)** The concentration response relationship was fitted to the Hill equation (solid line) to obtain the apparent K_m value of 30 ± 5μM for EAAC1(A334E) (solid circles) and 19 ± 8μM (wild type, open circles).

Figure 6: Steady-state transport is inhibited by the A334E mutation. **(A)** Typical current elicited by glutamate application through rapid solution exchange indicted by the bar at 0 mV showing transient outward currents but absence of steady-state response. The experiment was performed in the forward transport mode (inset) with 140 mM NaMES external and 140 mM KMES internal buffer (V = 0 mV). **(B)** I-V relationship for EAAC1(A334E) (red squares) and EAAC1(WT) (black squares) under conditions as in (A). **(C)** L-[^{3}H] glutamate uptake as a function of time for the wild-type transporter (squares) and the A334E-mutant transporter (circles) The values have been corrected for the uptake by cells transfected with the empty vector. **(D and E)** The distribution of the membrane potential along the membrane normal was computed for EAAC1(A334E) by solution of the Poisson-Boltzmann equation for the outward-facing (D) and inward facing (E) configuration. The arrow indicates the position of the A334E side chain in the mutated transporter. The black lines represent isopotential lines spaced at 20 mV from 0 mV to -100 mV. The color-coded scale of the membrane potential is indicated by the colored bar to the right of (E) (blue = 0 mV, grey = -50 mV, red = -100 mV). **(F)** Valence of the outward- to inward-facing transition.

Figure 7: Molecular dynamics (MD) simulations show structural distortion and increased water penetration into the "bowl" caused by the A334E mutation near HP1. **(A, B)** Structure near the tip of HP1 for EAAC1(WT) (A) and EAAC1(A334E) at the endpoint of 1 μs MD simulations.**(C, D)** Sudden increase of the distance between 334(Cα) and Asp(Cα) indicates substrate dissociation. Black red and blue traces indicate subunits 1, 2, and 3. **(E, F)** Radial distribution function for water as a function of the distance from 334(Cβ) demonstrates increased water penetration in A334E (F) vs. wild-type transporter (E) (after 1 μs simulation time).

Figure 8: [Na^+] dependence of glutamate-induced transient currents. **(A)** Typical transient currents (A334E) in response to glutamate application through photolysis of 2 mM MNI-caged glutamate at time t = 0 in the presence of 140 mM (black) or 20 mM (red) external sodium. **(B)** Charge obtained from integrating the current in (A). **(C)** Time constant for the relaxation of the outward current. All recordings were performed at V = 0 mV with NaMES (external) and 140 mM KMES (internal). At 20 mM Na^+, the solution was balanced with NMG^+ to a total cation concentration of 140 mM.

Figure 9: The double mutation A334E-R446Q abolishes the outward charge movement upon binding of a neutral substrate. **(A)** Current in response to rapid application of alanine by photolysis of MNI-caged alanine at time t = 0 (V = 0 mV, 140 mM NaMes external, 140 mM NaMes, 10 mM alanine

internal).**(B)** Concentration response relationship of anion current elicited by application of alanine (V = 0 mV, 140 mM NaMes external, 140 mM NaSCN, 10 mM alanine internal).

Figure 10: Sequential Na^+/substrate binding model explaining the experimental data. The model is based on previous results (40), as well as current data. T=transporter, S=substrate. The simulations for the wild-type transporter (green box) and A334E (red box) were performed as described previously (6,60), using numerical integration of the rate equations pertaining to the sequential binding mechanism. The kinetic parameters were estimated based on previous results. They do not provide a unique representation of the data, but can describe the experimental results well. The following parameters were used at V = 0 mV (wild type): Na^+ binding to the empty transporter: k_{for} = 20 $M^{-1}ms^{-1}$, k_{rev} = 1 ms^{-1}, z_Q = 0.4; Glutamate binding: k_{for} =10,000 $M^{-1}ms^{-1}$, k_{rev} = 1 ms^{-1}, z_Q = -0.16; Na^+ binding to the glutamate-bound transporter: k_{for} = 1 $M^{-1}ms^{-1}$, k_{rev} = 0.2 ms^{-1}, z_Q = 0.6; $TNa^+S \leftrightarrow T'Na^+S$: k_{for} = 5 $M^{-1}ms^{-1}$, k_{rev} = 0.1 ms^{-1}, z_Q = 0.4; [Glu] = 200 μM; [Na^+] = 0.14 M. For the A334E mutant transporter, k_{for} ($TNa^+S \leftrightarrow T'Na^+S$) was set to 0, with all other parameters kept at the same value. The apparent rate constant of glutamate release from the caged precursor was set to 2 ms^{-1}, accounting for the non-instantaneous rise of the outward current.

FIGURES

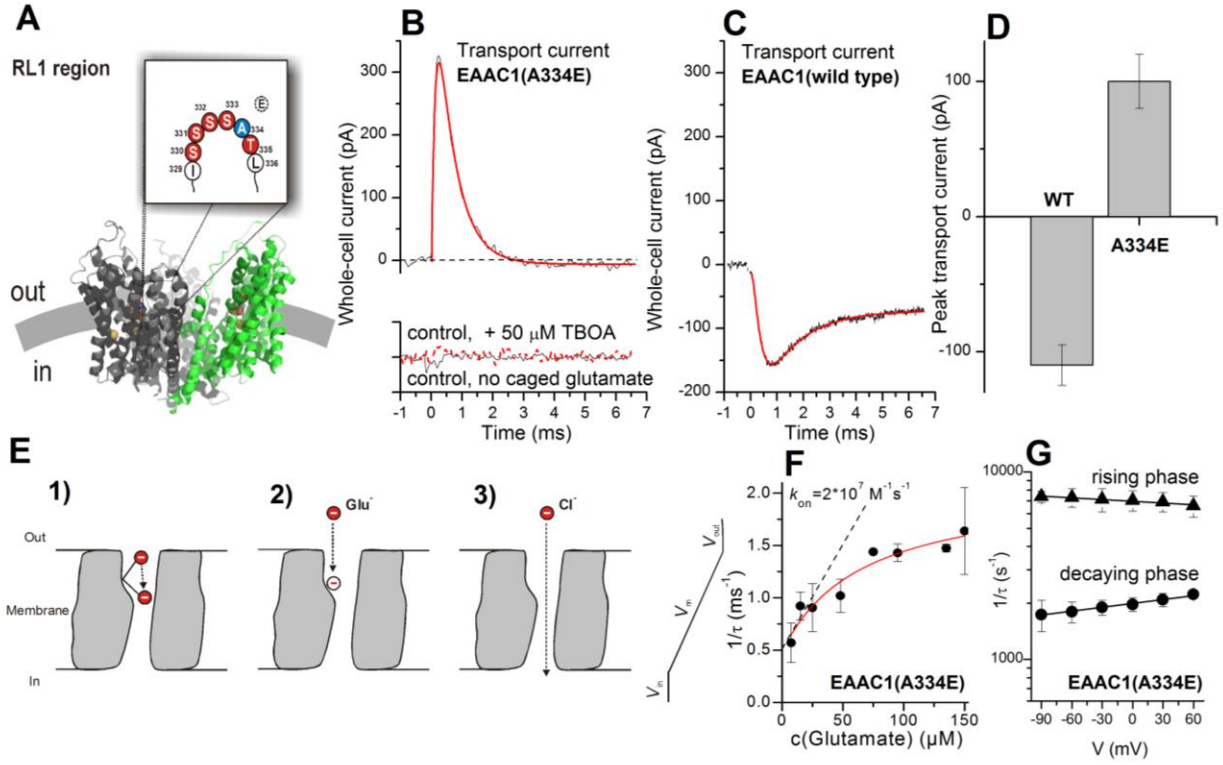

Figure 1

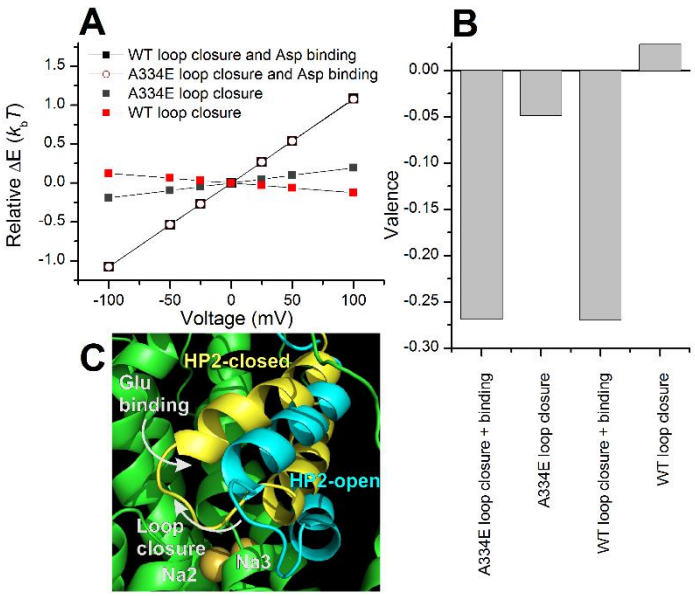

Figure 2

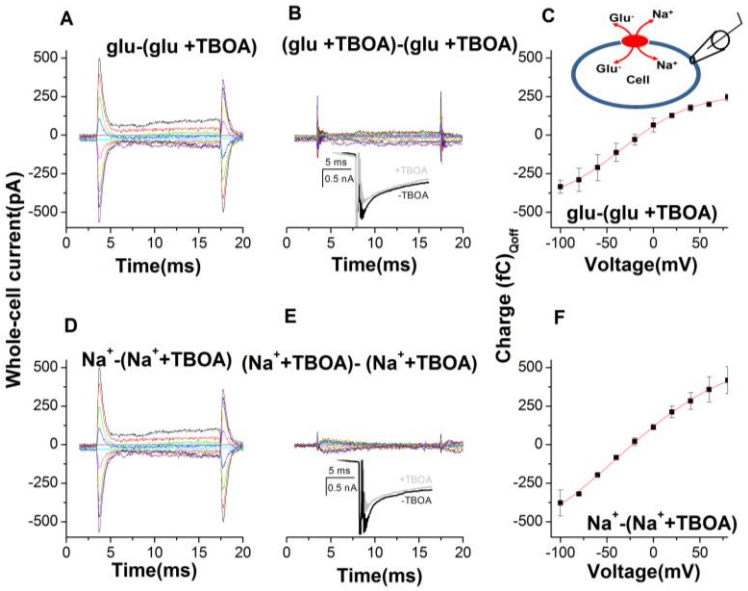

Figure 3

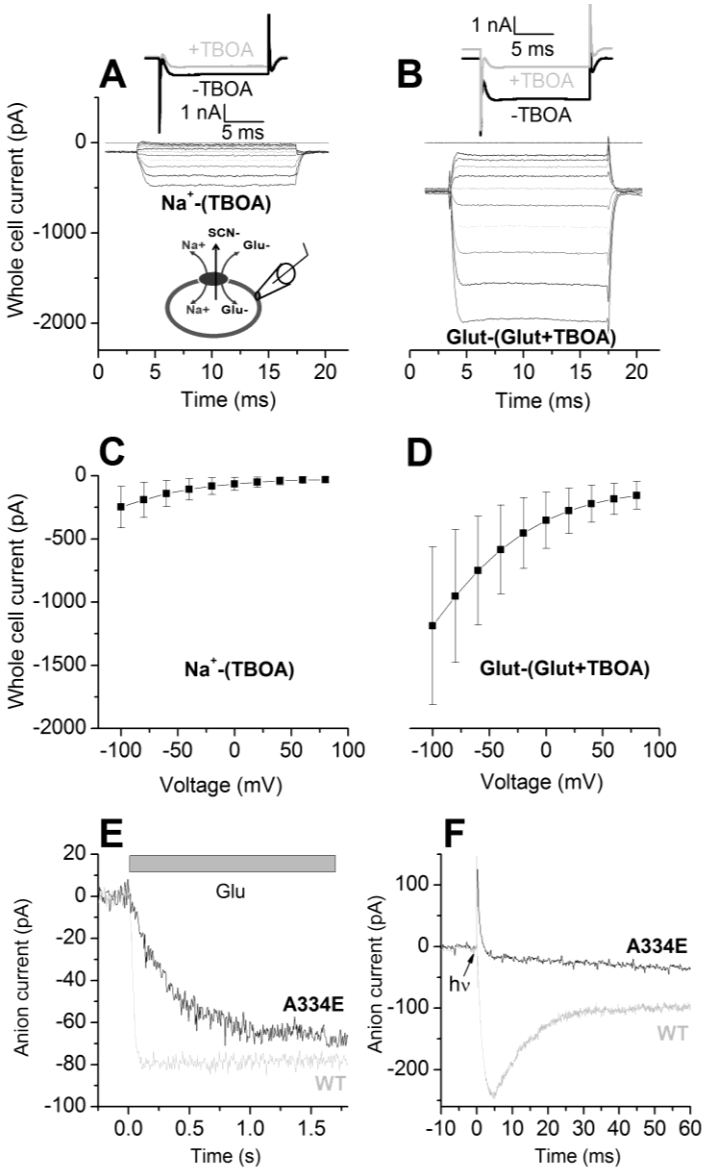

Figure 4

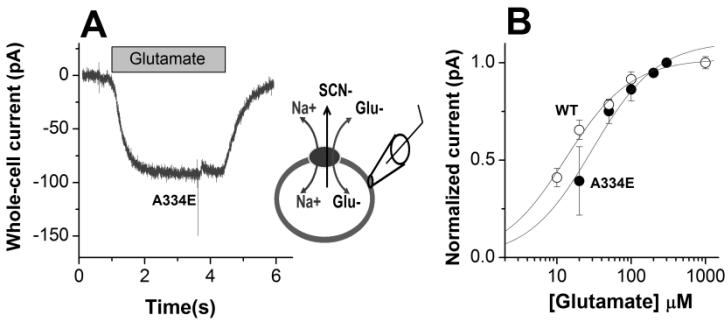

Figure 5

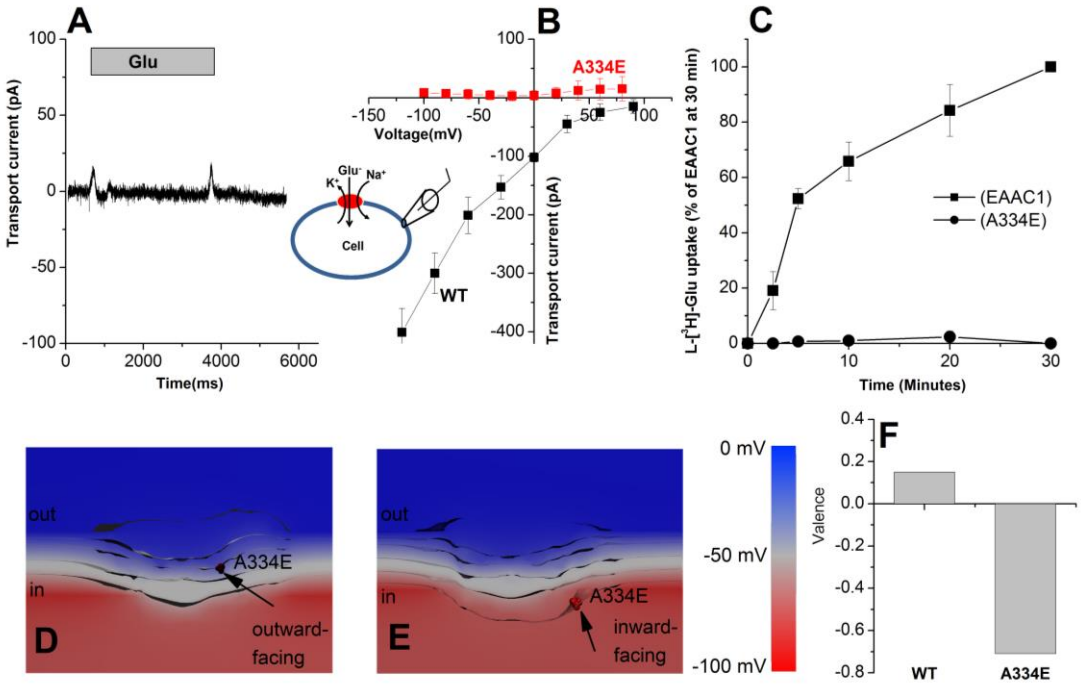

Figure 6

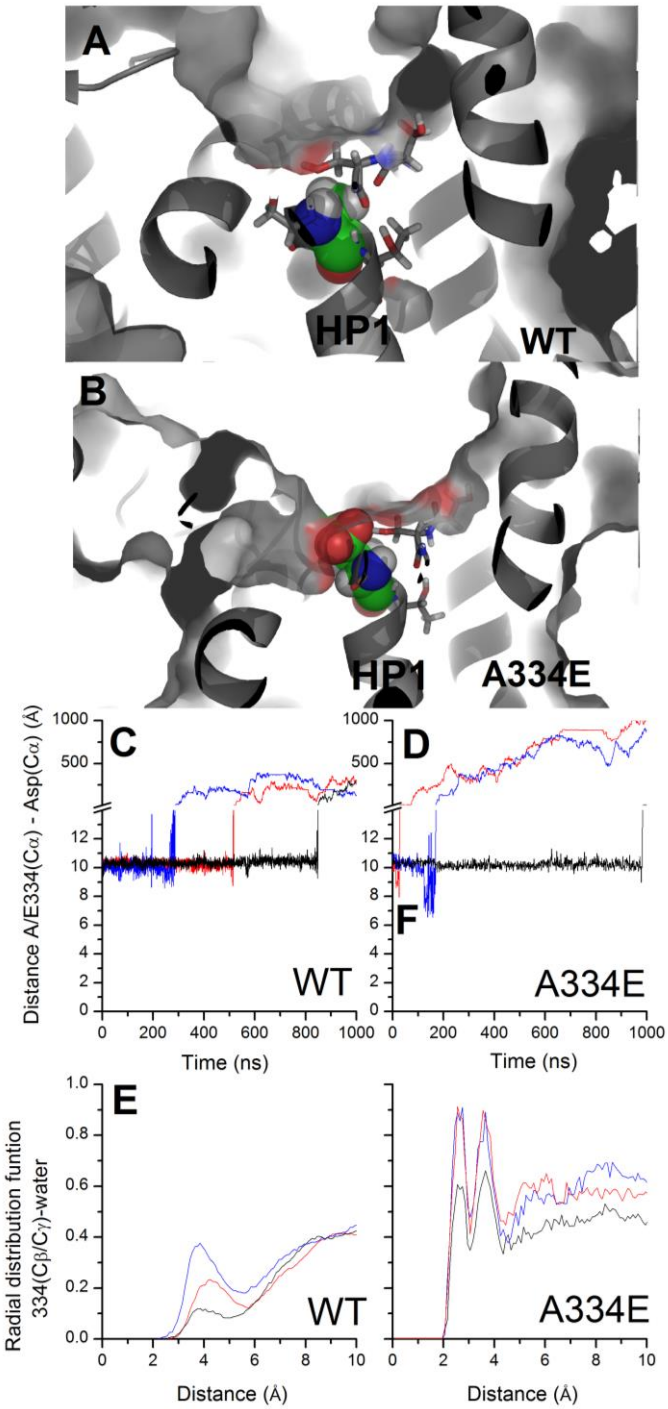

Figure 7

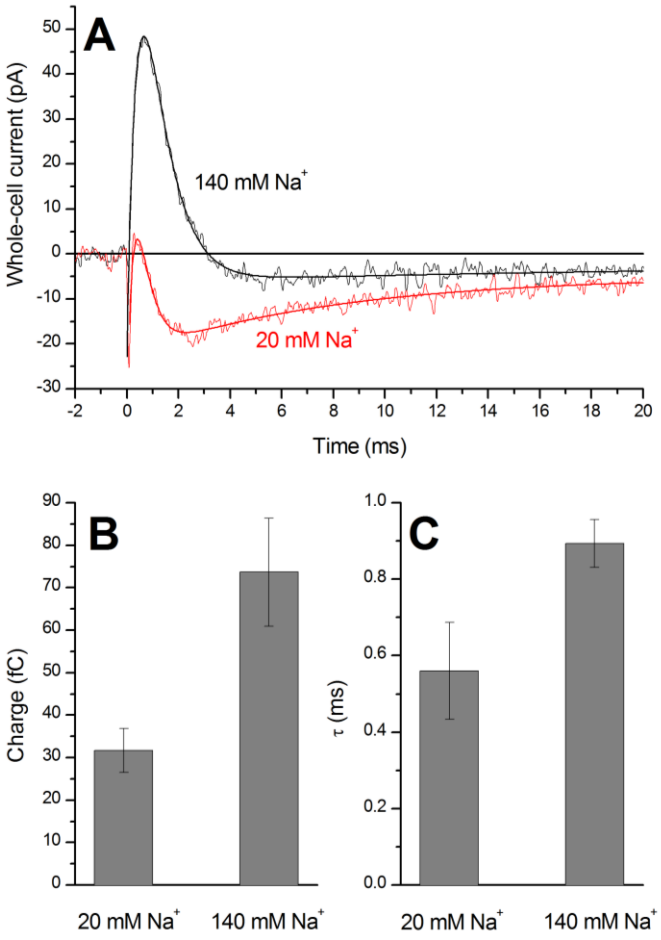

Figure 8

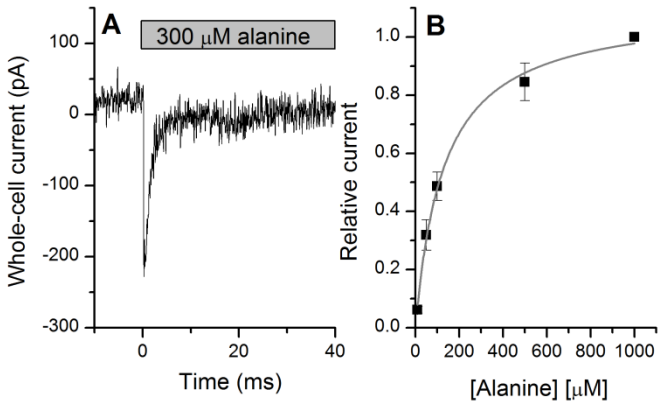

Figure 9

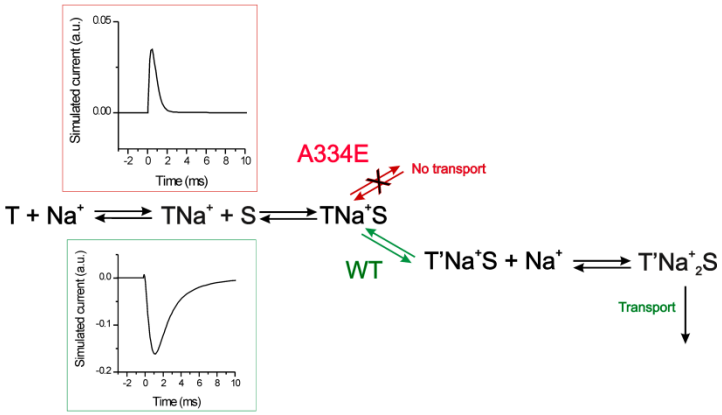

Figure 10

Electrogenic Steps Associated with Substrate Binding to the Neuronal Glutamate Transporter EAAC1

Rose Tanui, Zhen Tao, Nechama Silverstein, Baruch Kanner and Christof Grewer

J. Biol. Chem. published online April 4, 2016
